Applied Surface Science 506 (2020) 144768

Contents lists available at ScienceDirect

Applied Surface Science

journal homepage: www.elsevier.com/locate/apsusc

Full Length Article

The role of relative humidity on crystallization of calcium carbonate from calcium acetoacetate precursor

Andreja Pondelak[a], Francesca Rosi[d], Celeste Maurich[b], Costanza Miliani[e], Srečo D. Škapin[c], Andrijana Sever Škapin[a,*]

[a] Slovenian National Building and Civil Engineering Institute, Dimičeva 12, 1000 Ljubljana, Slovenia
[b] Istituto CNR di Scienze e Tecnologie Molecolari (CNR-ISTM), c/o, Via Elce di sotto 8, Perugia 06123 Italy
[c] Advanced Materials Department, Jožef Stefan Institute, Jamova 39, 1000 Ljubljana, Slovenia
[d] Istituto di Scienze e Tecnologie Chimiche Giulio Natta Consiglio Nazionale delle Ricerche (CNR-SCITEC), c/o via Elce di Sotto 8, 06123, Perugia, Italy
[e] Istituto di Scienze del Patrimonio Culturale Consiglio Nazionale delle Ricerche (CNR-ISPC), Via Guglielmo Sanfelice, 8-Naples, Italy

ARTICLE INFO

Keywords:
Calcium acetoacetate
Relative humidity
Carbonation
Amorphous carbonate
Vaterite
Mechanism

ABSTRACT

Calcium acetoacetate, $Ca(OAcAc)_2$, was exposed 7, 30 and 365 days to different values of relative humidity (33%, 48%, 75% and 96%) at 40 °C in order to study its transformation to $CaCO_3$. The resulting $Ca(OAcAc)_2$ decomposition and the time dependence of the phase transformations were monitored and critically evaluated by Fourier transform infrared spectroscopy, field emission scanning electron microscopy and X-ray powder diffraction. The impact of relative humidity on $CaCO_3$ polymorph formation was thoroughly assessed. In all of the conditions used and for all ageing periods, the formed crystal structure is found to be vaterite. At the lowest relative humidity (33%), the amorphous $CaCO_3$ remains more or less almost untransformed even after one year of exposure. It is proposed that the reason for the stability of amorphous $CaCO_3$ is due to the limited amount of physisorbed water on the surfaces of the particles, which is considered the driving force for its transformation. However, the carbonation process is faster in the case of the highest humidity (96%). The findings are not only important for better solutions in the field of cultural heritage, but also shed new light on the fundamental mechanism of $CaCO_3$ crystallization.

1. Introduction

Recently, the use of water-based solutions of calcium acetoacetate, $Ca(OAcAc)_2$, was proposed for the consolidation of mineral materials [1]. $Ca(OAcAc)_2$ in the presence of water or relative humidity (RH) decomposes to acetone, CO_2 and $CaCO_3$. Consolidation is achieved when the CO_2 and acetone evaporate and the newly formed $CaCO_3$ particles fill the substrate porosity.

$CaCO_3$ can be found in at least six different phases. Three anhydrous polymorphs: calcite, aragonite and vaterite and three hydrated forms: crystalline monohydrate – monohydrocalcite, ($CaCO_3{\cdot}H_2O$), crystalline hexahydrate – ikaite ($CaCO_3{\cdot}6H_2O$) and an amorphous $CaCO_3$ hydrate (ACC) [2,3]. Although there are known conditions that can influence the crystallization steps and, as a consequence, control the formation of the crystal phase, information of the influence of relative humidity on the precipitation and crystal habits of the different $CaCO_3$ polymorphs is very scarce. Ogino et al. [4] showed that ACC dispersed in water transforms into a mixture of several crystalline $CaCO_3$ polymorphs within several minutes, while its transformation in air is much slower. Xu et al. [5] studied the transformation of ACC into crystalline $CaCO_3$ and found that $CaCO_3$ with different morphologies, crystal phases and structures can be obtained by controlling the humidity and temperature. They found that by increasing the humidity, the dissolution-recrystallisation process of $CaCO_3$ is increased and therefore the rate of ACC crystallisation, since the solubility of ACC is higher than that of anhydrous crystalline forms. The research carried out by Konrad et al. [6] showed that the metastability of ACC is controlled by the availability of water during storage – removing physisorbed water prolonged the metastability and prevented transformation. It was reported by different authors that the crystallisation of ACC is strongly affected by water content [6–8].

There are literature reports on at least three mechanisms of ACC transformation into crystalline $CaCO_3$. In all three mechanisms, ACC first converts to vaterite and subsequently to calcite. The first

* Corresponding author at: Slovenian National Building and Civil Engineering Institute, Dimičeva 12, 1000 Ljubljana, Slovenia.
E-mail addresses: andreja.pondelak@zag.si (A. Pondelak), francesca.rosi@cnr.it (F. Rosi), celeste.maurich@libero.it (C. Maurich), costanza.miliani@cnr.it (C. Miliani), sreco.skapin@ijs.si (S.D. Škapin), andrijana.skapin@zag.si (A. Sever Škapin).

https://doi.org/10.1016/j.apsusc.2019.144768
Received 4 June 2019; Received in revised form 3 October 2019; Accepted 17 November 2019
Available online 29 November 2019

mechanism suggests that ACC dissolves and vaterite spheres are formed *via* homogeneous nucleation of nano-crystalline vaterite particles, followed by fast aggregation to form micrometre-sized polycrystalline spheres [9]. In the second mechanism, ACC particles first rapidly dehydrate and crystallise to form individual crystalline particles, followed by (partial) dissolution and re-precipitation [10–12]. Third, a recent mechanism suggests that vaterite forms *via* ACC dissolution coupled to spherulitic growth [13]. Spherulitic growth is a nucleation controlled process, driven by the high supersaturation levels, where new nuclei continuously form on the surface of the growing spherulite but with no structural relationship between the pre-existing and new particles [14–15]. On the other hand, only two mechanisms of transformation of vaterite or aragonite into calcite have been proposed: (a) solid-state transformation and (b) dissolution-re-crystallisation [5]. The first transformation occurs either by internal rearrangements of atoms, ions or molecules, while the second transformation occurs by dissolution of the metastable phase(s) in the solution with which this phase(s) is in contact and the simultaneous precipitation of the stable phase from the same solution [16].

The aim of this study is to assess the influence of RH on decomposition of $Ca(OAcAc)_2$ into $CaCO_3$. Hence, we exposed $Ca(OAcAc)_2$ to different RH and determine the rate of decomposition, identifying the phase of formed $CaCO_3$ of samples at different times. Additionally, the mechanism of $Ca(OAcAc)_2$ decomposition to amorphous $CaCO_3$ and its transformation to $CaCO_3$ crystalline phase(s) was proposed. Such findings provide knowledge about the consolidation process of newly proposed consolidant what is the crucial for successful protection of cultural heritage materials. For effective consolidation, it is essential to determine the optimum conditions for consolidating processes of porous carbonate-based materials, such as stones, mural paintings or sculptures. There are many researches on the synthesis and application of nanolime-based consolidants [2,3], but none of the research deals about the mechanism of $Ca(OAcAc)_2$ decomposition and its transformation to $CaCO_3$ as well as the effects of treatment conditions on this process.

2. Materials and methods

2.1. Materials and sample preparation

A water solution of $Ca(OAcAc)_2$, used in this study, is a recently proposed consolidant for reinforcing porous mineral materials. It was developed in the scope of HEROMAT FP7 project [17] and is described in detail in the patent [1]. $Ca(OAcAc)_2$ was 9.6 wt% (corresponding to 4% of theoretically formed $CaCO_3$). In a typical experiment, 10 g of the starting water solution of $Ca(OAcAc)_2$ (Fig. S1a, Supporting information) was placed into a uncovered Petri dish and dried for 3 days at room temperature (RT). Obtained dry product (Fig. S1b, Supporting information) was then homogenised (Fig. S1c, Supporting information) and then exposed in uncovered Petri dish for 7, 30 and 365 days to 40 °C, and 33%, 48%, 75% and 96% RH. Saturated salt solutions of $MgCl_2$ (33% RH), $Mg(NO_3)_2{\cdot}6H_2O$ (48%), NaCl (75%) and K_2SO_4 (96% RH) were used to control relative humidity. Before individual measurements the sample was additionally homogenised. In order to accelerate the process of decomposition of $Ca(OAcAc)_2$ the selected temperature for the study was 40 °C (at RT the process can last even few years). High content of initial component $Ca(OAcAc)_2$ was ensured by drying its water solution at RT for 3 days before examination.

2.2. Analytical techniques and experimental procedures

Fourier transform infrared spectroscopy (FT-IR) was used to investigate the $Ca(OAcAc)_2$ decomposition rate and to identify the newly formed $CaCO_3$ phase(s) at different exposure time intervals and RHs. FT-IR spectra were recorded with a Perkin Elmer Spectrum 100 FT-IR spectrophotometer in the region 4000–375 cm^{-1}, with a spectral resolution of 4 cm^{-1} and 64 scans. Spectra were acquired in transmission mode through KBr pellets containing ~1 mg of the sample in 120 mg KBr. In order to achieve sample homogeneity each individual sample was mixed before FT-IR measurements using agate pestle and mortar.

The morphology and size of the obtained $CaCO_3$ particles were investigated using a Field emission scanning electron microscope (FESEM) (Zeiss ULTRA plus) equipped with an energy-dispersive spectrometer (EDXS, Oxford Instruments). An InLens detector was used. The samples were placed on double sided carbon tape and additionally Pt-coated prior to examination using Gatan, PECS, Model 682. The thickness of Pt coating was 3 nm.

X-ray powder diffraction (XRD) was performed to identify different crystalline polymorphs of the obtained $CaCO_3$ particles. Analyses were performed by using D4 Endeavor, Bruker AXS with Cu Kα radiation (λ = 0.154 nm) and Sol-X detector. The measurements of powdered samples were done in a 2 theta range of 20–70° with a scanning step of 0.02° and 3 s counting time per step. Scherrer equation was used for the determination of the crystallite size of $CaCO_3$ particles:

$$\tau = \frac{K\lambda}{\beta\cos\theta} \quad (1)$$

where τ is the mean size of the ordered (crystalline) domains, K is a dimensionless shape factor, λ is the X-ray wavelength, β is the line broadening at half the maximum intensity (FWHM) and θ is the Bragg angle.

3. Results and discussion

3.1. Characterisation of $Ca(OAcAc)_2$

Fig. 1 shows the FT-IR spectrum of starting dry $Ca(OAcAc)_2$ (before it was placed in the climatic chambers) in the region between 4000 cm^{-1} and 375 cm^{-1}. Characteristic bands for $Ca(OAcAc)_2$ and amorphous $CaCO_3$ in Fig. 1 are marked with asterisks * and ACC, respectively. The strong band at 1709 cm^{-1} belongs to C═O symmetric stretching (ν_s[C═O]), bands at 1580 cm^{-1} and 1419 cm^{-1} may include both the C═O and C═C stretching of the enol form of $Ca(OAcAc)_2$ and the COO^- anti-symmetric and symmetric stretching ($\nu_{as}[COO^-]$ at 1580 cm^{-1} and $\nu_s[COO^-]$ at 1419 cm^{-1}). The band at 1419 cm^{-1} can be attributed to $Ca(OAcAc)_2$ compound or ACC as well because of bands overlapping and the band shifting. Bands in the 3000–2800 cm^{-1} range are due to CH stretching. Bands in the region 1300 cm^{-1} to 900 cm^{-1} include C—O and C—C stretchings and CH bendings. In the region below 900 cm^{-1}, the corresponding C—C and C—O bending and rocking modes are located.

In addition to the bands characteristic for $Ca(OAcAc)_2$, bands at 1493 cm^{-1}, 865 cm^{-1} and the absence of a medium intensity band around 700 cm^{-1} indicate the occurrence of amorphous $CaCO_3$ (Fig. 1 with abbreviation ACC) [10,18,19]. The band at 1493 cm^{-1} is due to the anti-symmetric stretching of CO_3^{-2} group (ν_3), the band at 865 cm^{-1} is associated with the out-of-plane bending vibrations of CO_3^{-2} group (ν_2), while the band at 690 cm^{-1} is due to in-plane bending vibrations of the CO_3^{-2} group (ν_4), in which ACC is weaker and broader with respect to the crystalline forms of $CaCO_3$. More information about the attribution of bands 1419 cm^{-1} and 1493 cm^{-1} is explained in detail in Supporting information. FESEM image in Fig. 2a shows that dry $Ca(OAcAc)_2$ has the shape of amorphous film; non-crystallinity was determined by XRD (Fig. 2b).

3.2. The effect of different humidity on the rate of transformation and polymorph formations

The principle of consolidation with the new consolidant,

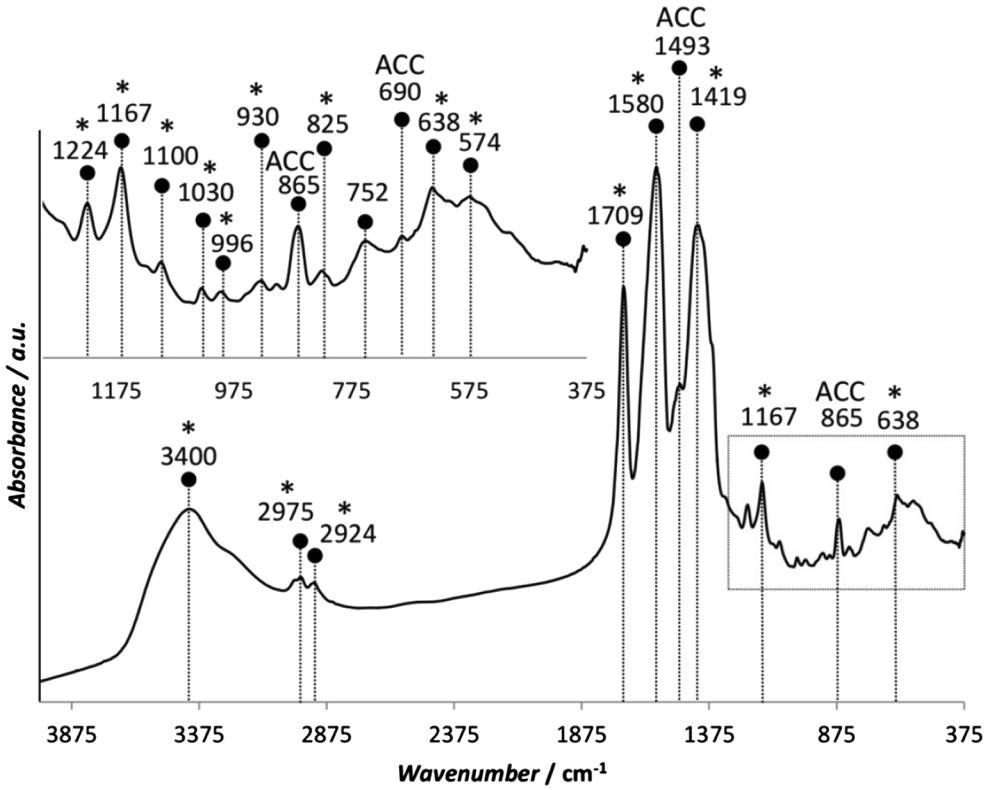

Fig. 1. FT-IR spectrum of a dry $Ca(OAcAc)_2$ sample: water solution of $Ca(OAcAc)_2$ exposed 3 days at room temperature; * – $Ca(OAcAc)_2$, ACC – amorphous $CaCO_3$.

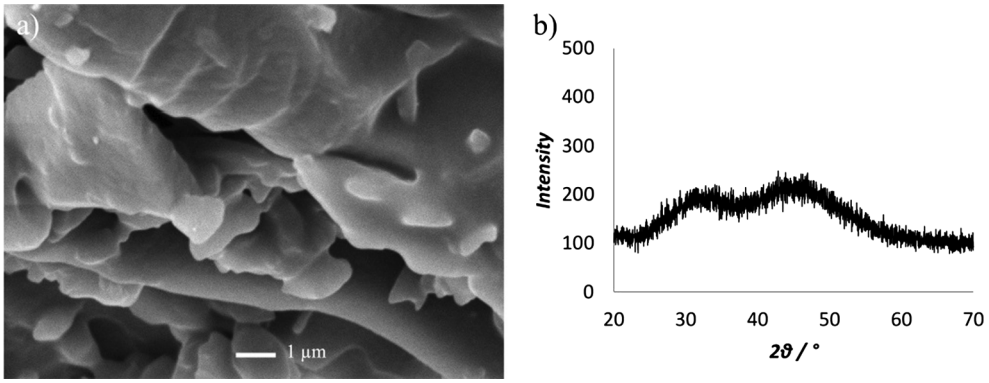

Fig. 2. SEM micrograph (a) and XRD pattern (b) of dry $Ca(OAcAc)_2$ sample.

$Ca(OAcAc)_2$, is the reaction (1) of spontaneous decarboxylation of $Ca(OAcAc)_2$ in the presence of water, producing acetone, calcium carbonate and CO_2 [1]:

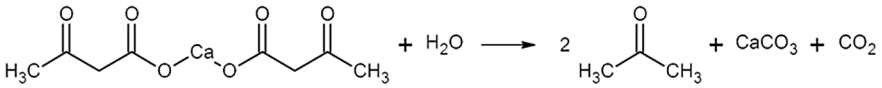

(1)

The rate of decarboxylation of $Ca(OAcAc)_2$ is greatly influenced by the treatment conditions, such as temperature and relative humidity.

In order to assess the influence of RH on $Ca(OAcAc)_2$ decomposition and carbonate phases transformations, the FT-IR spectra of samples cured at 33%, 48%, 75% and 96% RH were collected at different time intervals (7 and 30 days in the case of samples exposed to all RHs and additional 365 days for samples exposed to the lowest and highest RHs). FT-IR spectra of samples exposed 7 and 30 days to all RHs (33%, 48%, 75% and 96%) are presented in Fig. 3a and b. For better presentation the FT-IR spectra of samples exposed 7, 30 and 365 days to the lowest (33%) and highest (96%) RH is presented in Fig. 4a and b.

The decomposition of $Ca(OAcAc)_2$ was followed by observing the decrease in $Ca(OAcAc)_2$ bands. Observing the general trend, it is noted that at the initial stage (7 and 30 days) of curing, $Ca(OAcAc)_2$ bands diminish faster in the sample exposed to the lowest RH (33%) than in the samples exposed to higher RHs (48%, 75% and 96%) (Fig. 3a and b). After one year it can be clearly seen that $Ca(OAcAc)_2$ is still present in the sample exposed to lowest RH (33%) (Fig. 4a), while in the case of sample exposed to the highest RH (96%) the decomposition reaches completion, showing no bands assigned to the starting material (Fig. 4b).

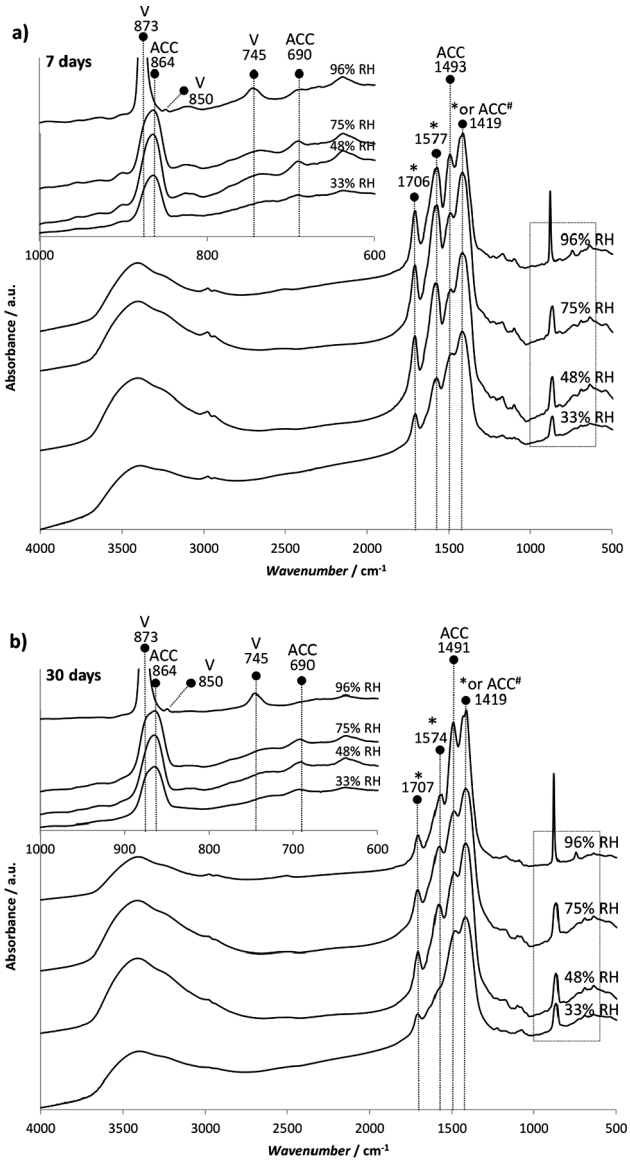

Fig. 3. FT-IR spectra of the sample exposed: (a) 7 and (b) 30 days at 33%, 48%, 75% and 96% RH at 40 °C. The insert shows an enlargement of the 1000–600 cm^{-1} region. #Note that due to the band shifting and overlapping the band at 1419 cm^{-1} (a and b) may be attributed to $Ca(OAcAc)_2$ or ACC.

The decomposition of the starting material is accompanied by the formation of $CaCO_3$. The distinction of the different $CaCO_3$ phases is possible by evaluating the low wavenumber range of the FT-IR spectrum. The main $CaCO_3$ phase found in the sample exposed for 7 days to 33%, 48% and 75% RH is ACC. As reported before, this is indicated by the broad band at 864 cm^{-1}, by the presence of band at 1493 cm^{-1} and by the absence of a medium band at about 700 cm^{-1} (marked with ACC in Figs. 3a and 4a) [10,18,19]. The band at 1493 cm^{-1} can be attributed to ACC and V as well. More information about that is explained in Supporting information. After 30 days, the main component in all samples exposed to 33%, 48% and 75% RH is ACC indicating that the transformation of ACC into crystalline $CaCO_3$ is slow at 33%, 48% and 75% RH. On the other hand, the sample, exposed to the highest RH (96%), clearly shows a band linked to a crystalline phase vaterite already after 7 days and remains untransformed after 365 days of exposure (Fig. 4b). The presence of a doublet at about 1493 cm^{-1} and

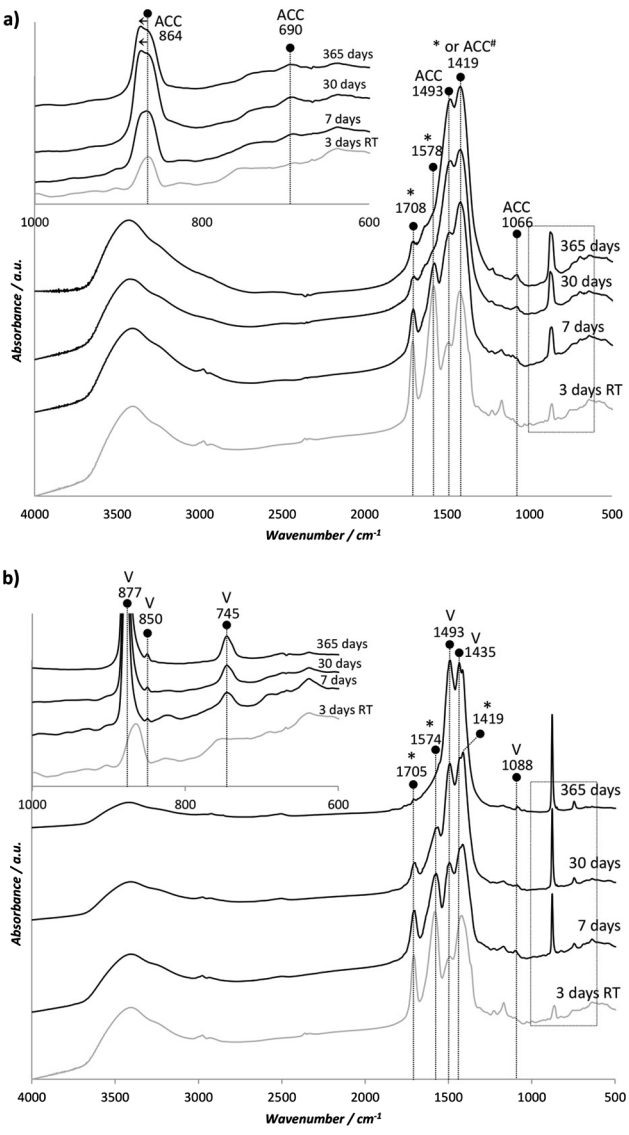

Fig. 4. FT-IR spectra of the sample exposed 7, 30 and 365 days at 40 °C and: (a) 33% and (b) 96% RH. The insert shows an enlargement of the 1000–600 cm^{-1} region. As a reference, the FT-IR spectrum of the sample exposed for 3 days at RT is added and designated with lighter line. #Note that due to the band shifting and overlapping the band at 1419 cm^{-1} (a) may be attributed to Ca $(OAcAc)_2$ or ACC. Arrows in (a) indicate shifting of band at 864 cm^{-1} towards higher wavenumbers, suggesting slight transformation of ACC to V.

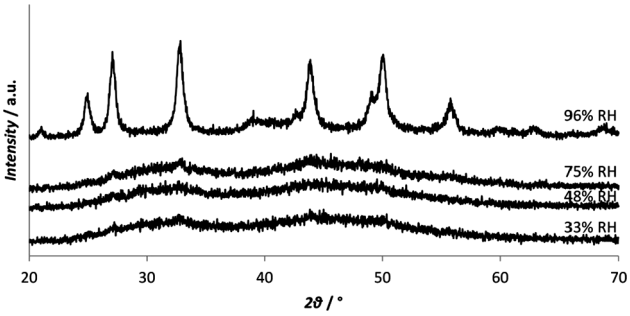

Fig. 5. XRD patterns of samples exposed 30 days to: 33% RH, 48% RH, 75% RH and 96% RH. Curves follow from the lowest to the highest relative humidity up.

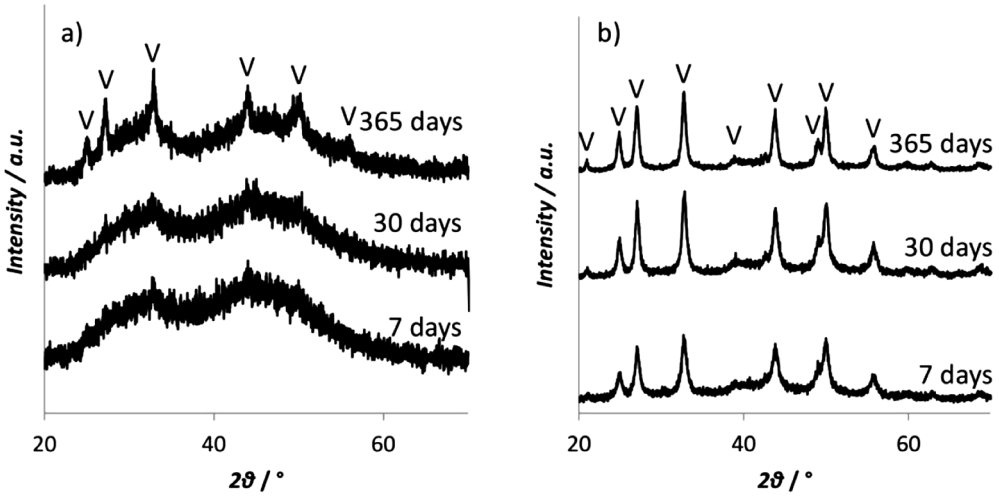

Fig. 6. XRD patterns of samples exposed 7, 30 and 365 days to: (a) 33% RH and (b) 96% RH.

Table 1
Summary of the characterization results of samples exposed for 7, 30 and 365 days to 33% RH and 96% RH.

RH (%)	Time (days)	$CaCO_3$ phase	Particle shape	Particle size	
				Primary (nm)	Aggregate[$] (μm)
33	7	ACC	Monolithic surface with origins of nanostructure	15–60[$]	N/d
33	30	ACC	Monolithic surface with origins of nanostructure and formation of spherical shaped particles	15–30[$]	2–5
33	365	ACC	Nanoparticles which are merging together into half-spheres and/or into spherical aggregates	15–20[$]	2–3
96	7	V	Nanoparticles which are merging into spherical aggregates	13[#]	s: 0.2–0.4
96	30	V	Nanoparticles which are merging into spherical and polygonal aggregates	15[#]	s: 0.2–0.5 b: 1–3
96	365	V	Nanoparticles which are merging into polygonal aggregates	17[#]	s: 0.3–0.5 b: 1–3

N/d – no detected.
ACC – amorphous $CaCO_3$.
V – vaterite.
s – smaller particles.
b – bigger particles.
[$] Estimated values obtained from FESEM micrographs.
[#] Estimated values calculated using the Scherrer equation.

1435 cm^{-1} representing the ν_3 mode, along with the corresponding ν_2 mode split at 877–850 cm^{-1} clearly indicate the occurrence of a non-centrosymmetric structure like vaterite [20].

FT-IR results are confirmed by XRD results, presented in Figs. 5 and 6a, b. Samples exposed for 7 and 30 days to 33%, 48% and 75% RH contain ACC phase, showing broad humps with poorly developed peaks of vaterite (Figs. 5 and 6a). The XRD pattern of samples exposed for 365 days to 33% RH shows defined diffraction peaks (Fig. 6a – the highest pattern), characteristic for vaterite, indicating higher crystallinity. The XRD results suggest the presence of only vaterite as the crystalline phase of the sample exposed 7, 30 and 365 days to 96% RH (Figs. 5 and 6b).

These findings clearly show a significant influence of RH both on the $Ca(OAcAc)_2$ decomposition and on the conversion of the ACC phase into vaterite crystalline phase. Low RH values (33%) limit the decomposition of the starting material, still present after one year, and the conversion of ACC to crystalline $CaCO_3$. On the contrary, higher RH values (96%) favour the $Ca(OAcAc)_2$ decomposition, leading to the total consumption of the starting material and the formation of ACC, which transforms to vaterite already after 7 days of exposure.

These results suggest that high humidity conditions would benefit the conversion of the ACC phase into vaterite when applying the water solution of $Ca(OAcAc)_2$ in the real case scenarios. According to the kinetic results of the $Ca(OAcAc)_2$ decomposition the consolidation process cannot be achieved within one month after application.

In this study, the only crystalline phase formed from ACC is vaterite, which did not transform into calcite or aragonite crystals, even after 365 days of exposure to high RH. Vaterite is a metastable phase, which easily and irreversibly converts into one of the more thermodynamically stable phases of $CaCO_3$ (aragonite or calcite) [16]. It is reported [4] that vaterite in water at 30 °C fully transforms into calcite in approximately 370 min, while at 50 °C vaterite converts into aragonite in approximately 60 min and further into calcite by approximately 900 min. The transformation of vaterite into other more thermodynamically stable phases of $CaCO_3$ may be hindered by the limited transport of moisture in air (environment in the present study) with respect to that which can happen in water. Moreover, it is possible that the presence of an organic component [21–23], which is $Ca(OAcAc)_2$ in the original system studied, and/or the presence of sulphates and/or phosphates [13,24], stabilise or more probably promote the stabilisation of the vaterite phase. Organic components may act as a template for vaterite heterogeneous nucleation, or they can inhibit the transition from metastable to stable phases [21].

The formed types of $CaCO_3$ phase, morphology and dimensions of the formed primary particles of selected samples are presented in Table 1. The primary particle size of crystallised samples coincided well with the crystallite size, which were measured with FESEM and by XRD using Scherrer equation, respectively. In Fig. S2a, c, e (Supporting

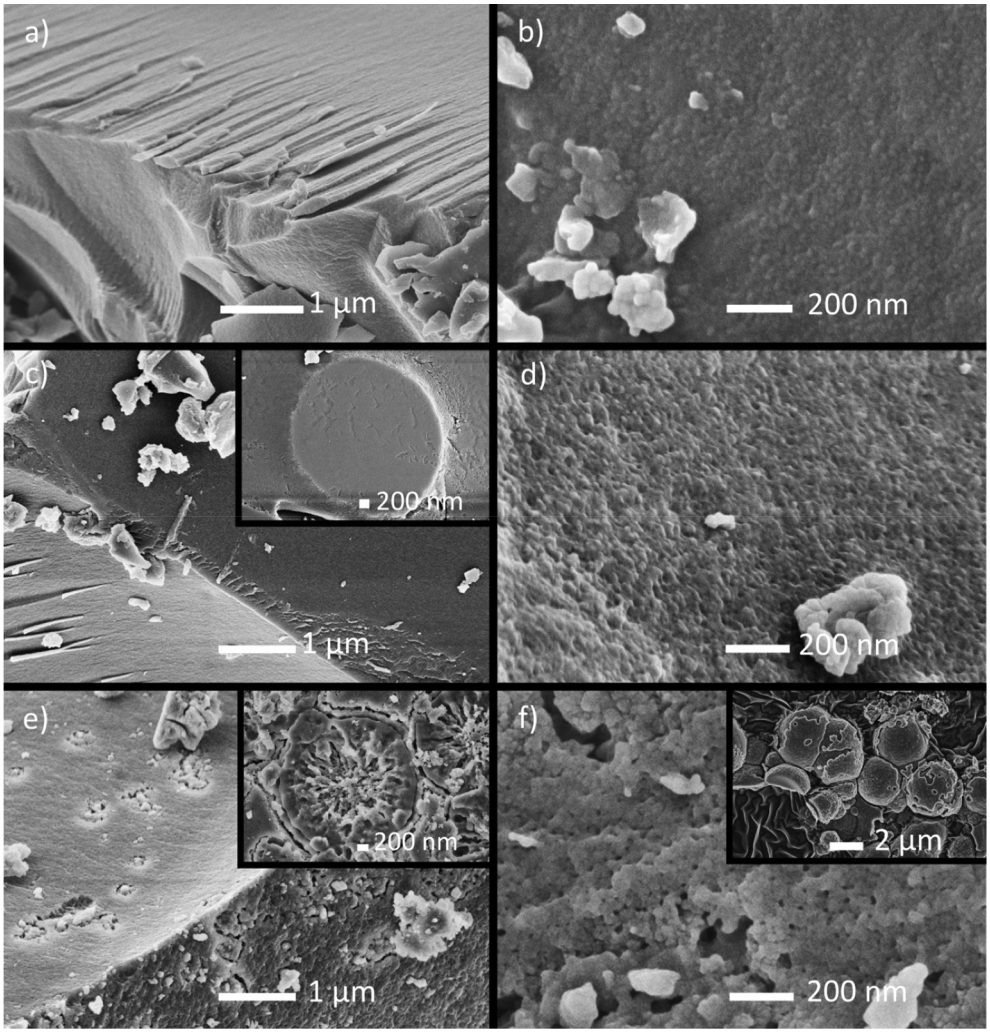

Fig. 7. FESEM images of samples exposed: (a, b) 7, (c, d) 30 and (e, f) 365 days to 33% RH.

information) the FESEM images of the samples exposed to 33% RH are shown, which provide a basis for the estimation of primary particle size. The estimated size of the primary particles obtained from FESEM micrographs for samples, exposed for 7, 30 and 365 days to 33% RH, is presented in Table 1. Diameters of the primary vaterite particles calculated from the Scherrer equation for the samples exposed to 96% RH are between 13 nm and 17 nm (Table 1). These values of primary particles coincide with the results obtained by FESEM images presented in Fig. S2b, d, f (Supporting information) where the obtained diameter of primary vaterite particles was between 13 nm and 40 nm.

The overall results indicate that the size of the primary particles is about the same, regardless of the sample being exposed to the lowest or highest values of RH. Vaterite nanoparticles, formed at 96% RH, are transformed from amorphous $CaCO_3$ nanoparticles and do not form directly form $Ca(OAcAc)_2$ since after only three days at RT the only $CaCO_3$ phase found by FTIR is ACC (Fig. 1). A similar finding was reported by Xu et al. [25], who showed that the morphology and size of vaterite nanoparticles are similar to the particles of ACC, which indicates that the ACC phase has a key role in the formation of vaterite nanoparticles.

FESEM images of sample exposed 7 days to 33% RH (Fig. 7a and b) show a monolithic surface of $Ca(OAcAc)_2$ (Fig. 7a) in which nano-structured ACC starts to form (Fig. 7b). After prolonged exposure (30 days), along with the poorly defined structure of nano-structured ACC (Fig. 7c and d) spherical shaped particles (Fig. 7c insert image), most likely the beginning of vaterite aggregates, are also visible. After even prolonged exposure (365 days) of the sample to the same conditions, the monolithic film composed from ACC nanoparticles is still present (Fig. 7e and f). However, some of these ACC nanoparticles have been transformed into vaterite nanoparticles and have merged into larger partly or crystalline vaterite (i.e. semi-crystalline) aggregates of rounded shape (Fig. 7e and insert image in the same figure). This is in agreement with the mechanism proposed by Ihli et al. [12] on the ACC-vaterite transformation. The conversion results from the dehydration and partial dissolution of the ACC phase in nanoparticles and agglomerates followed by the re-crystallisation of the ACC phase into vaterite nanoparticles. These semi-crystalline vaterite particles most likely merge together to form spherical vaterite, with a size between 2 µm and 3 µm, as shown in Fig. 7f (insert image).

In agreement with the previous results, the sample exposed for 7 days to 96% RH is already composed of vaterite in the form of spherical aggregates, with a diameter of approximately 200 nm to 400 nm (Fig. 8a). The presence of original $Ca(OAcAc)_2$ is evidenced by the film which surrounds vaterite aggregates (shown in Fig. 8a with arrows), since the structure is similar to the original material ($Ca(OAcAc)_2$) presented in Fig. 2a. Thirty days after sample preparation, this film is no longer visible, suggesting the consistent decrease in the quantity of $Ca(OAcAc)_2$. At this time, the rearrangement of vaterite nanoparticles occurs, appearing as aggregate particles with spherical to polygonal shape, with a diameter of approximately 200 nm to 500 nm (Fig. 8b). After prolonged exposure (365 days), the sample contains only vaterite aggregates of polygonal shape (Fig. 8c), ranging in size

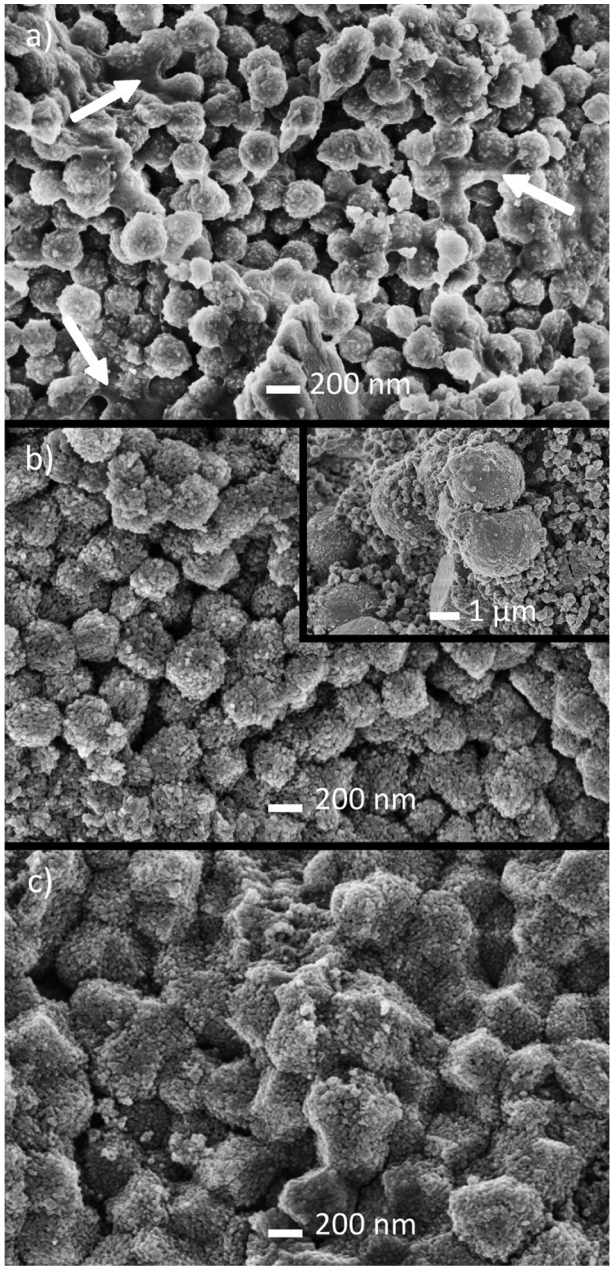

Fig. 8. FESEM images of samples exposed: (a) 7, (b) 30 and (c) 365 days to 96% RH. Arrows indicates undecomposed $Ca(OAcAc)_2$.

from 300 nm to 500 nm, suggesting the further rearrangement of vaterite nanoparticles. As shown in the inserted image in Figs. 8b and S3 (Supporting information), samples exposed for 30 and 365 days also contain larger aggregated particles, with a diameter between 1 µm and 3 µm. The growth of these particles can be attributed to Ostwald's ripening [26], which explains the passage of mass from the smaller to larger particles, since the solubility of the smaller particles is larger in the absorbed water film. The particle size obtained in this study is consistent with the results reported by Brečević et al. [27]. They obtained spherical vaterite aggregates with the average size of 3 µm, which are composed of primary particles in the range of 20–35 nm.

According to Konrad et al. [6] the transformation of ACC into crystalline $CaCO_3$ in air is due the physisorbed water on the surface of ACC particles. Crystallisation is trigged only when a critical value of water is obtained and takes place *via* partial dissolution and re-precipitation. Although researchers did not prove that the ACC phase dissolves in water, it seems that diffusion transport of calcium and carbonate ions within aqueous layers is a necessary condition for the transformation of the ACC phase into the crystalline form. The study [6] also showed that the transformation of ACC to crystalline phases occurs only when a critical amount of physisorbed water is reached on the surface of the ACC phase. According to the FESEM image present in Fig. S4 (Supporting information), the transformation of ACC to vaterite particles takes place only on the surface (aggregates of rounded shape). It seems that only on the surface where water is available the formation of vaterite can take place. Moreover, the crystallisation of ACC to other crystalline phases is slow and progressive at low RH. Water availability is undoubtedly a parameter which controls the transformation of ACC into crystalline forms.

It is concluded that during real case scenarios (i.e. application on cultural heritage objects) it is likely that variation in the relative humidity in the area where water solution of $Ca(OAcAc)_2$ is applied would contribute to formation of vaterite modification. We found out the long term stability of vaterite in our systems, despite it is known [4] that calcite is a thermodynamically the most stable phase of crystalline $CaCO_3$.

3.3. The proposed mechanism of $Ca(OAcAc)_2$ decomposition and the formation of $CaCO_3$ particles

The proposed mechanism of decomposition of $Ca(OAcAc)_2$ and the formation of $CaCO_3$ particles of sample exposed to low RH (33%) is presented in Fig. 9. $Ca(OAcAc)_2$ exposed to 40 °C and to moisture in the air decomposes to ACC nanoparticles. Water is adsorbed on the surfaces of formed ACC nanoparticles. Here, based on the results of Konrad et al. [6] ACC dissolves and re-precipitates only when a critical amount of water is physisorbed on the amorphous carbonate nanoparticles. This leads to integration of nanoparticles into spherical particles [5,6,10,11].

The proposed mechanism of the decomposition of $Ca(OAcAc)_2$ and the formation of $CaCO_3$ particles for samples exposed to high RH (96%) is presented in Fig. 10. Compared to the samples exposed to lower RH, samples at higher RH quickly reach the critical value of water physisorbed onto the surfaces of $CaCO_3$ nanoparticles and can therefore convert to vaterite more rapidly, as shown schematically in Fig. 9. Formed vaterite nanoparticles then merge into aggregates through the nano-aggregation mechanism. Furthermore, the particles rearrange and grow due to Ostwald's ripening, which lead to larger particles of polygonal forms. Vaterite particles can be formed by the spherulitic growth [13]. Although the formation of vaterite according to this mechanism is likely, since vaterite particles on FESEM image in Fig. S5a and b (Supporting information), show a characteristic radiation-like array of crystalline subunits. It is more likely that the mechanism of the formation of vaterite particles is nano-aggregation and not the spherulitic growth. Beck et al. [15] suggest that in the case of nano-aggregation the uniform size of primary nano-particles is observed, what is in accordance with the results presented in the present paper (uniform size of primary particles in Fig. S2b, d, f, Supporting Information). Moreover, the progression of noncrystallographic branching would be observed as a function of time, supplying direct visual evidence for spherulitic growth [15]. The size of primary particles does not change after time (see Table 1), what is the additional evidence that nano-aggregation is more likely the mechanism.

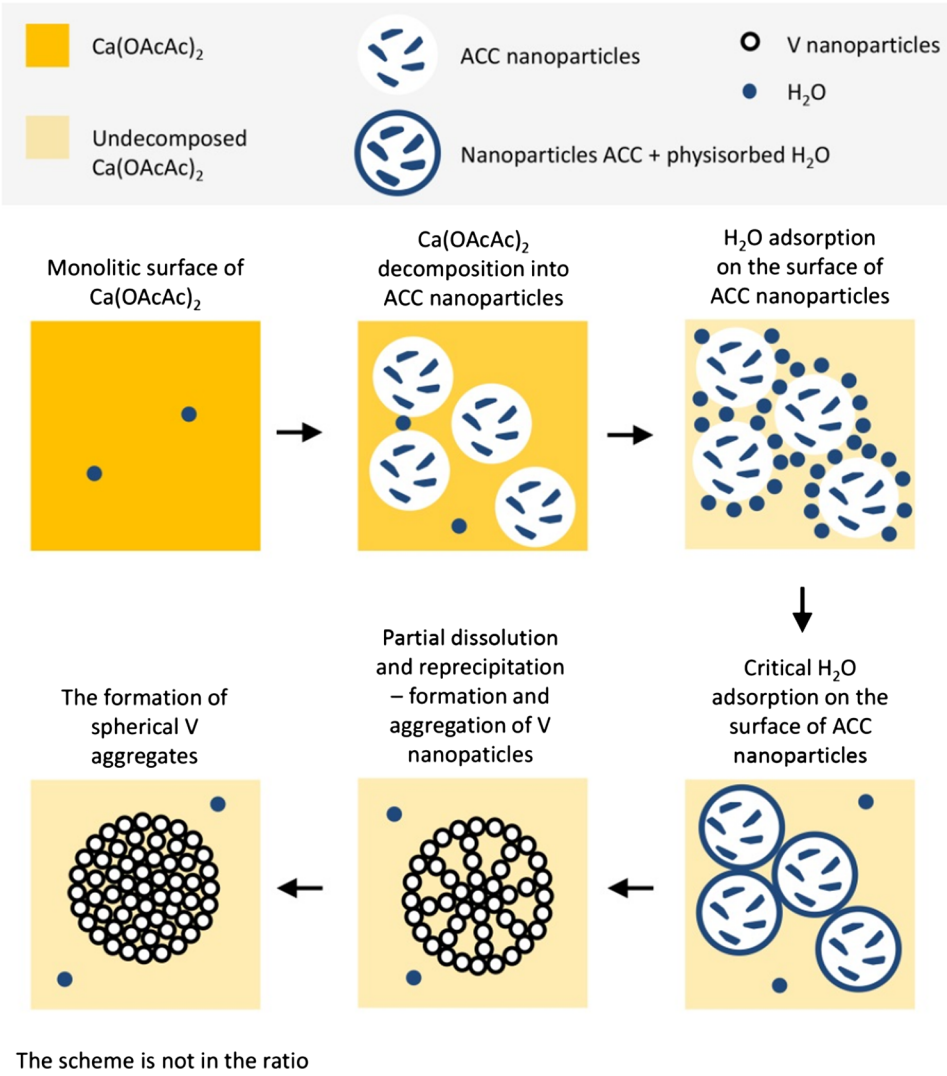

Fig. 9. Schematic illustration of $Ca(OAcAc)_2$ decomposition and transformation of amorphous $CaCO_3$ (ACC) into vaterite (V) of the samples exposed to lower RH (33%).

4. Conclusions

The paper describes the influence of relative humidity at 40 °C on calcium acetoacetate decomposition and $CaCO_3$ formation.

After one year of exposure of calcium acetoacetate to different relative humidity, the decomposition is incomplete for samples exposed to the lowest relative humidity (33%), while the decomposition is almost complete in the case samples have been exposed to the highest relative humidity (96%). Strong influence of relative humidity on $CaCO_3$ polymorph formation has been shown. At lower relative humidity amorphous $CaCO_3$ is still the main component of the sample even after one year exposure, while at the highest relative humidity (96%) the obtained $CaCO_3$ is in vaterite phase already after 7 days after exposure. Stability of amorphous $CaCO_3$ is associated with limited physisorbed water on the surface of the particles and is considered the necessary condition for the transformation of the amorphous $CaCO_3$ into crystalline form.

The proposed mechanism of calcium acetoacetate decomposition of samples exposed to low relative humidity (33%) is as follows. In the presence of the moisture from the air and at 40 °C, calcium acetoacetate decomposes to amorphous $CaCO_3$ nanoparticles. When the critical value of physisorbed water on the surface of particles is reached, the amorphous nanoparticles transforms into vaterite nanoparticles *via* dehydration, partial dissolution and the re-precipitation. This is followed by merging vaterite nanoparticles into spherical aggregates. In the case of a calcium acetoacetate sample exposed to high relative humidity (96%), we propose that vaterite nanoparticles are formed by rapid transformation of amorphous $CaCO_3$ since the critical value of physisorbed water on particles is quickly reached. Further vaterite nanoparticles merge into aggregates through the nano-aggregation mechanism. Prolonged exposure time leads to rearrangement and the growth of aggregates (Ostwald ripering), leading to larger particles of polygonal shape. Due to the uniform size of primary nano-particles which does not change after time it can be concluded that nano-aggregation is more likely the mechanism of the formation of vaterite particles.

From the practical point of view it can be concluded that consolidation process of treated historic material is faster if exposed to

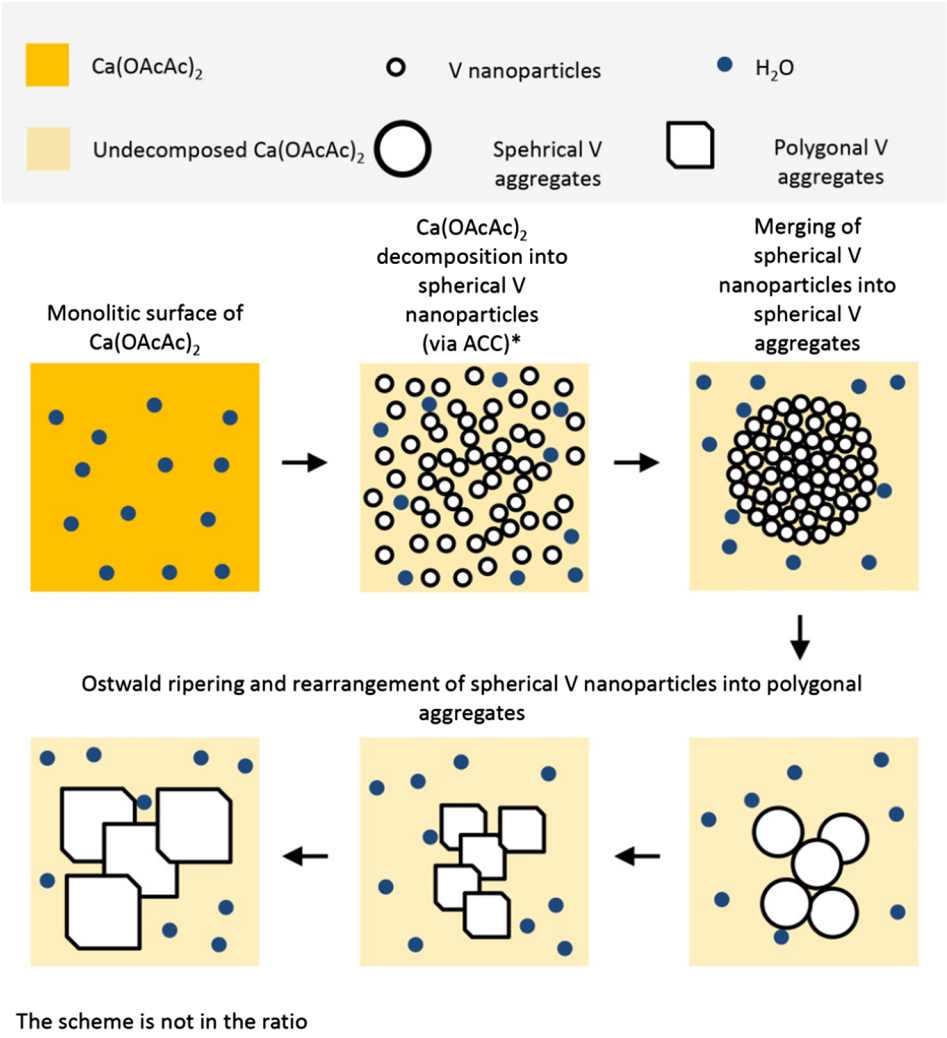

Fig. 10. Schematic illustration of $Ca(OAcAc)_2$ decomposition and transformation of amorphous $CaCO_3$ (ACC) into vaterite (V) of the samples exposed to higher RH (96%). * shows the proposed formation of V through ACC, as depicted in Fig. 9.

higher values of relative humidity. Carbonation kinetics determines the time frame for achieving the intended consolidation effect of consolidant. The results have significant impact on understanding of consolidation process of newly proposed consolidant based on calcium acetoacetate.

Declaration of Competing Interest

The authors declare that they have no known competing financial interests or personal relationships that could have appeared to influence the work reported in this paper.

Acknowledgements

The research leading to these results has received funding from the Slovenian Research Agency (No. Z4-9298, P2-0273).

Appendix A. Supplementary material

Supplementary data to this article can be found online at https://doi.org/10.1016/j.apsusc.2019.144768.

References

[1] L. Škrlep, A. Pondelak, A. Sever Škapin, Method for reinforcing porous construction materials and use calcium acetoacetate solution to this aim, Patent EP 3004028 (B1), 2017.
[2] L.S. Gomez-Villalba, P. Lopez-Arce, R. Fort, Nucleation of $CaCO_3$ polymorphs from a colloidal alcoholic solution of $Ca(OH)_2$ nanocrystals exposed to low humidity conditions, Appl. Phys. A 106 (2012) 213–217.
[3] P. Lopez-Arce, L.S. Gomez-Villalba, S. Martinez-Ramirez, M.A. de Buergo, R. Fort, Influence of relative humidity on the carbonation of calcium hydroxide nanoparticles and the formation of calcium carbonate polymorphs, Powder Technol. 205 (2011) 263–269.
[4] T. Ogino, T. Suzuki, K. Sawada, The formation and transformation mechanism of calcium carbonate in water, Geochim. Cosmochim. Acta 51 (1987) 2757–2767.
[5] X. Xu, J.T. Han, D.H. Kim, K. Cho, Two modes of transformation of amorphous calcium carbonate films in air, J. Phys. Chem. B 110 (2006) 2764–2770.
[6] F. Konrad, F. Gallien, D.E. Gerard, M. Dietzel, Transformation of amorphous calcium carbonate in air, Cryst. Growth Des. 16 (2016) 6310–6317.
[7] M. Albéric, L. Bertinetti, Z. Zou, P. Fratzl, W. Habraken, Y. Politi, The crystallization of amorphous calcium carbonate is kinetically governed by ion impurities and water, Adv. Sci. 5 (2018) 1701000.
[8] S. Leukel, W. Tremel, Water-controlled crystallization of $CaCO_3$, $SrCO_3$, and $MnCO_3$ from amorphous precursors, Cryst. Growth Des. 18 (2018) 4662–4670.
[9] R. Vacassy, J. Lemaitre, H. Hofmann, J.H. Gerlings, Calcium carbonate precipitation using new segmented flow tubular reactor, Aiche J. 46 (2000) 1241–1252.
[10] J.D. Rodriguez-Blanco, S. Shaw, L.G. Benning, The kinetics and mechanisms of amorphous calcium carbonate (ACC) crystallisation to calcite, via vaterite, Nanoscale 3 (2011) 265–271.
[11] C. Rodriguez-Navarro, K. Kudlacz, O. Cizer, E. Ruiz-Agudo, Formation of amorphous calcium carbonate and its transformation into mesostructured calcite, CrystEngComm 17 (2015) 58–72.
[12] J. Ihli, W.C. Wong, E.H. Noel, Y.Y. Kim, A.N. Kulak, H.K. Christenson, M.J. Duer, F.C. Meldrum, Dehydration and crystallization of amorphous calcium carbonate in solution and in air, Nat. Commun. 5 (2014) 1–10.
[13] P. Bots, L.G. Benning, J.D. Rodriguez-Blanco, T. Roncal-Herrero, S. Shaw, Mechanistic insights into the crystallisation of amorphous calcium carbonate (ACC),

Cryst. Growth Des. 12 (2012) 3806–3814.
[14] D.J. Tobler, J.D.R. Blanco, K. Dideriksen, K.K. Sand, N. Bovet, L.G. Benning, S.L.S. Stipp, The effect of aspartic acid and glycine on amorphous calcium carbonate (ACC) structure, stability and crystallization, Proc. Earth. Plan. Sci. 10 (2014) 143–148.
[15] R. Beck, J.P. Andreassen, Spherulitic growth of calcium carbonate, Cryst. Growth Des. 10 (2010) 2934–2947.
[16] L. Brečević, D. Kralj, On calcium carbonates: from fundamental research to application, Croat. Chem. Acta 80 (2007) 467–484.
[17] Protection of Cultural Heritage Objects with Multifunctional Advanced Materials, granted by the European Commission in the Seventh Framework Programme (2007–2013), Grand agreement No. 282992. http://www.heromat.com/ (accessed 19 October 2018).
[18] F.A. Andersen, L. Brecevic, Infrared spectra of amorphous and crystalline calcium carbonate, Acta Chem. Scand. 45 (1991) 1018–1024.
[19] E. Beniash, J. Aizenberg, L. Addadi, S. Weiner, Amorphous calcium carbonate transforms into calcite during sea urchin larval spicule growth, Proc. R. Soc. Lond. B 264 (1997) 461–465.
[20] W.B. White, The carbonate minerals, in: V.C. Farmer (Ed.), The Infrared Spectra of Minerals, Mineralogical Society, London, 1974, pp. 227–284.
[21] C. Rodriguez-Navarro, C. Jimenez-Lopez, A. Rodriguez-Navarro, M.T. Gonzalez-Munoz, M. Rodriguez-Gallego, Bacterially mediated mineralisation of vaterite, Geochim. Cosmochim. Acta 71 (2007) 1197–1213.
[22] J. Ihli, Y.Y. Kim, E.H. Noel, F.C. Meldrum, The effect of additives on amorphous calcium carbonate (ACC): Janus behaviour in solution and the solid state, Adv. Funct. Mater. 23 (2013) 1575–1585.
[23] R.S.K. Lam, J.M. Charnock, A. Lennie, F.C. Meldrum, Synthesis-dependent structural variations in amorphous calcium carbonate, CrystEngComm 9 (2007) 1226–1236.
[24] A. Katsifaras, N. Spanos, Effect of inorganic phosphate ions on the spontaneous precipitation of vaterite and on the transformation of vaterite to calcite, J. Cryst. Growth 204 (1999) 183–190.
[25] S.J. Xu, P.Y. Wu, Monodisperse spherical $CaCO_3$ superstructure self-assembled by vaterite lamella under control of regenerated silk fibroin via compressed CO_2, CrystEngComm 15 (2013) 5179–5188.
[26] J. Prah, J. Maček, G. Drazić, Precipitation of calcium carbonate from a calcium acetate and ammonium carbamate batch system, J. Cryst. Growth 324 (2011) 229–234.
[27] L. Brečević, V. NothigLaslo, D. Kralj, S. Popovič, Effect of divalent cations on the formation and structure of calcium carbonate polymorphs, J. Chem. Soc. 92 (1996) 1017–1022.